

Supporting Information

Self-aligned stitching growth of centimeter-scale quasi-single-crystalline hexagonal boron nitride monolayers on liquid copper

Qing Zhang,^a Huixin Chen,^a Suilin Liu,^b Yinyin Yu,^a Cuiru Wang,^a Jian Han,^c Guosheng Shao,^a and Zhiqiang Yao^{,a}*

^aSchool of Materials Science and Engineering, State Centre for International Cooperation on Designer Low Carbon and Environmental Material, Zhengzhou University, Zhengzhou 450001, China

^bAnalytical and Testing Center, Sichuan University, Chengdu 610064, China.

^cNational Engineering Research Centre for Advanced Polymer Processing Technology, Zhengzhou University, Zhengzhou 450003, China.

*Corresponding Author: zqyao@zzu.edu.cn (Z. Yao)

Table of Contents:

Figure S1. a) Photograph of the original Cu foil used for hBN growth. b) Schematic procedure for hBN growth on liquid Cu surfaces.

Figure S2. Fractal clustering growth of hBN on liquid Cu. a) Schematic illustration of the one-tube APCVD furnace used in initial hBN growths. b) SEM image of the as-grown sample.

Figure S3. Effect of sublimation temperature of ammonia borane precursor (T_{NB}) on morphology and alignment of hBN domains grown on liquid Cu by DTC APCVD. a-d) SEM images of hBN domains grown under different T_{NB} of 60 °C, 70 °C, 80 °C, 90 °C, respectively.

Figure S4. Effect of H₂ content on morphology and alignment of hBN domains grown on liquid Cu by DTC APCVD. a-d) SEM images of hBN domains grown as a function of H₂ content of 0% (Ar/H₂=500:0 sccm), 4.8% (500:25 sccm), 7.4% (500:40 sccm), 10.7% (500:60 sccm), respectively.

Figure S5. Effect of growth temperature on collimation behavior of merged hBN grains grown on liquid Cu by DTC APCVD. a-b) Optical images of merged domains grown at lower temperatures of 1098 °C and 1090 °C, respectively. c-d) Atomic models for seamless stitching and seam stitching from adjacent domains, respectively.

Figure S6. Microstructure of annealed Cu and resolidified Cu. a) SEM image, c) EBSD IPF mapping, e) SAED and g) XRD patterns of annealed polycrystalline Cu. b) SEM image, d) EBSD IPF mapping, f) SAED and h) XRD patterns of resolidified single crystalline Cu.

Figure S7. Nonuniform growth of hBN on annealed Cu. a) Schematic procedure for hBN growth on annealed polycrystalline Cu by DTC APCVD. b and c) Optical images of hBN domains grown preferentially along the defect sites of rough grooves and uneven rolling surfaces on annealed polycrystalline Cu, respectively.

Figure S8. Misorientated growth of hBN on resolidified Cu. a) Schematic procedure for hBN growth on resolidified Cu by DTC APCVD. b and c) Optical images of hBN domains and films grown on resolidified Cu, respectively.

Figure S9. Stoichiometry of B and N in hBN film grown on liquid Cu by DTC APCVD. a) Survey XPS spectrum, b) B 1s and N 1s core level spectra. The inset in a) shows the optical image of the transferred hBN film on SiO₂/Si for XPS measurement.

Figure S10. UV-Vis absorption spectrum of the transferred hBN film on quartz plate. The inset shows the plot of $(ah\nu)^2$ versus $h\nu$, by which the optical band gap of 6.0 eV for hBN film is determined.

Figure S11. HRTEM images of the regions numbered 1-5 in Fig. 3a. The insets in each image show the corresponding fast Fourier transform patterns.

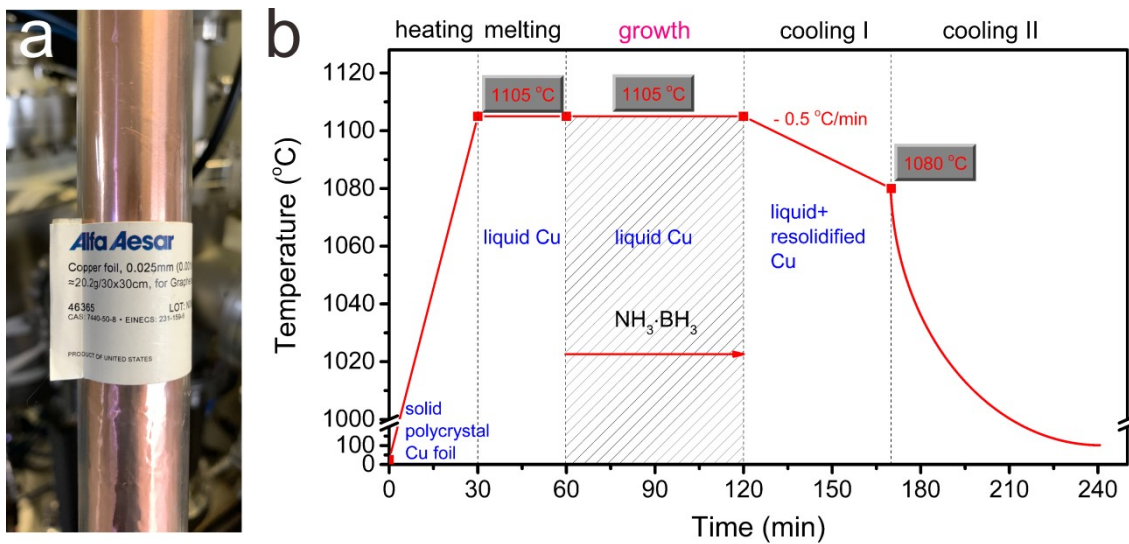


Figure S1. a) Photograph of the original Cu foil used for hBN growth. b) Schematic procedure for hBN growth on liquid Cu surfaces.

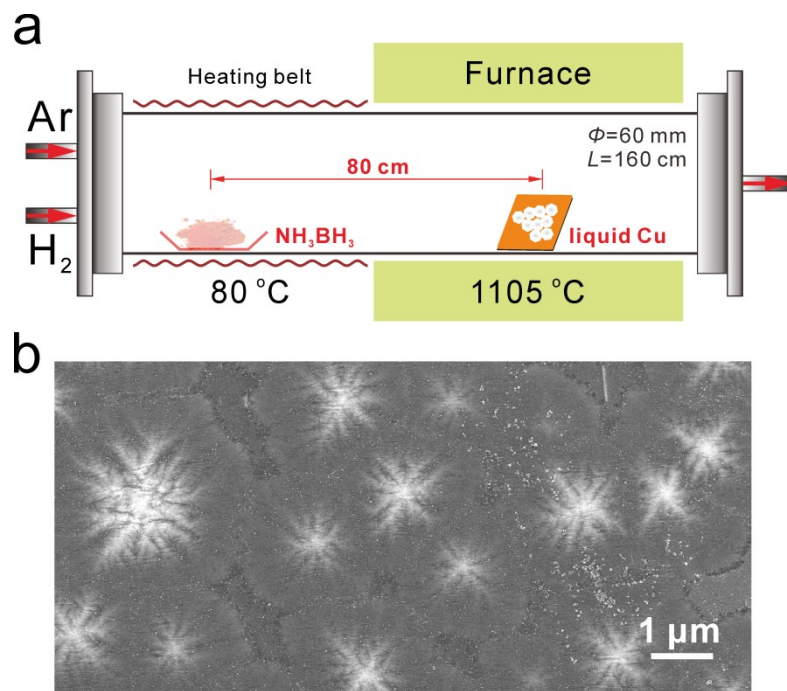


Figure S2. Fractal clustering growth of hBN on liquid Cu. a) Schematic illustration of the one-tube APCVD furnace used in initial hBN growths. b) SEM image of the as-grown sample.

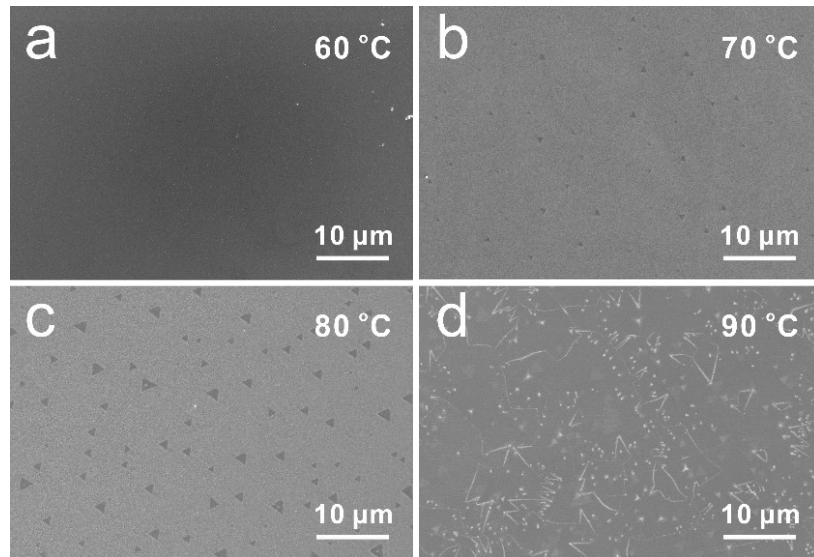


Figure S3. Effect of sublimation temperature of ammonia borane precursor (T_{NB}) on morphology and alignment of hBN domains grown on liquid Cu by DTC APCVD. a-d) SEM images of hBN domains grown under different T_{NB} of 60 °C, 70 °C, 80 °C, 90 °C, respectively.

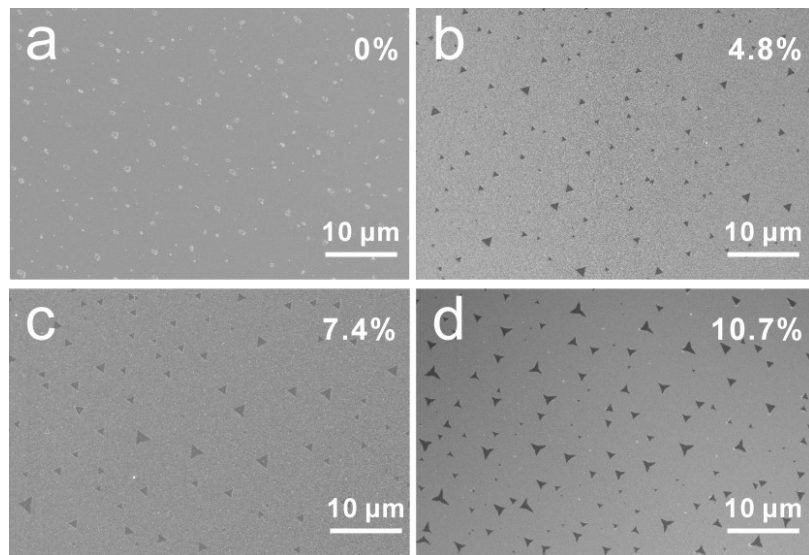


Figure S4. Effect of H₂ content on morphology and alignment of hBN domains grown on liquid Cu by DTC APCVD. a-d) SEM images of hBN domains grown as a function of H₂ content of 0% (Ar/H₂=500:0 sccm), 4.8% (500:25 sccm), 7.4% (500:40 sccm), 10.7% (500:60 sccm), respectively.

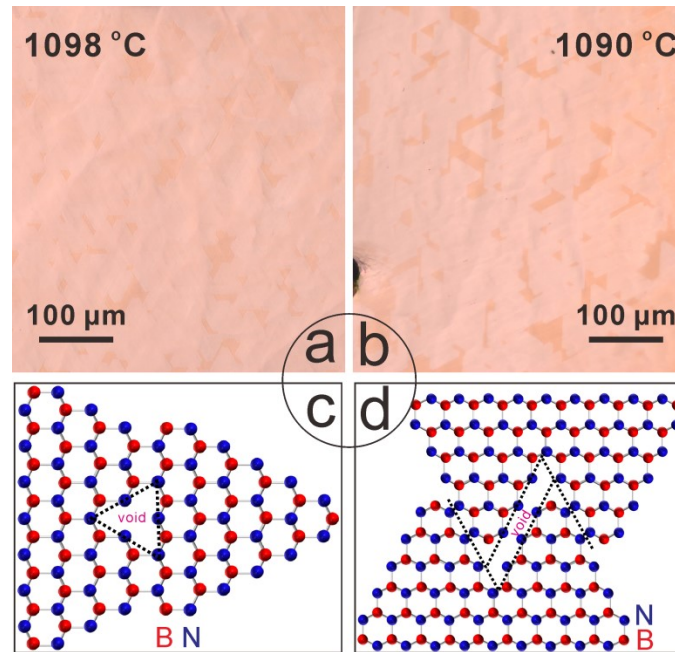


Figure S5. Effect of growth temperature on collimation behavior of merged hBN grains grown on liquid Cu by DTC APCVD. a-b) Optical images of merged domains grown at lower temperatures of 1098 °C and 1090 °C, respectively. c-d) Atomic models for seamless stitching and seam stitching from adjacent domains, respectively.

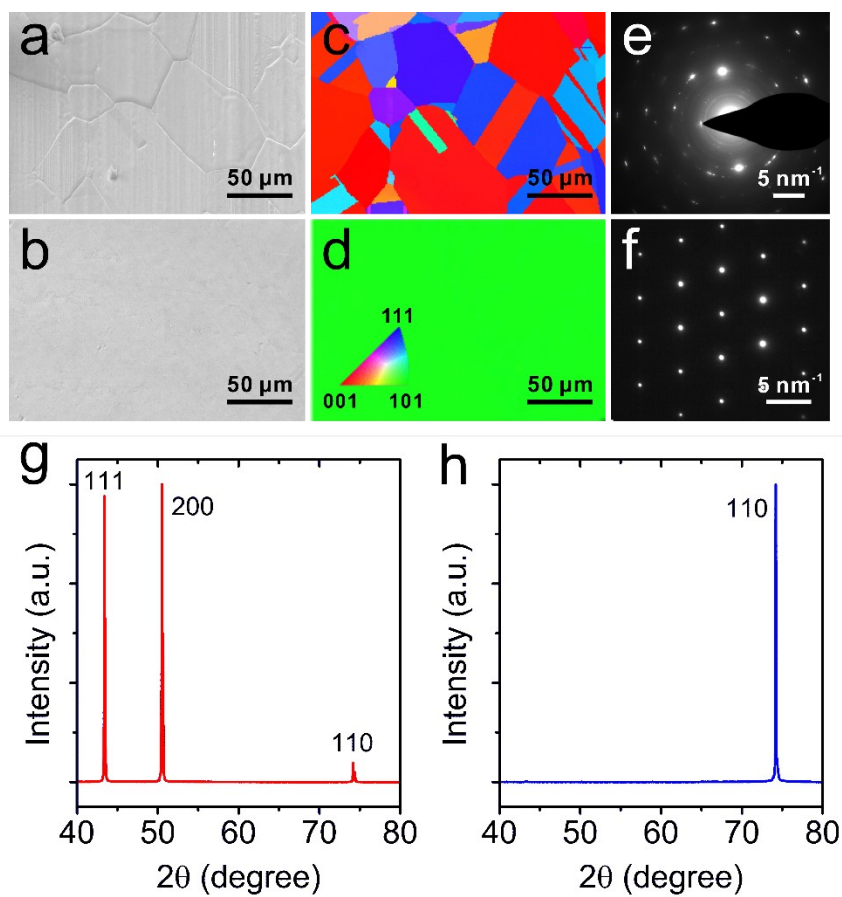


Figure S6. Microstructure of annealed Cu and resolidified Cu. a) SEM image, c) EBSD IPF mapping, e) SAED and g) XRD patterns of annealed polycrystalline Cu. b) SEM image, d) EBSD IPF mapping, f) SAED and h) XRD patterns of resolidified single crystalline Cu.

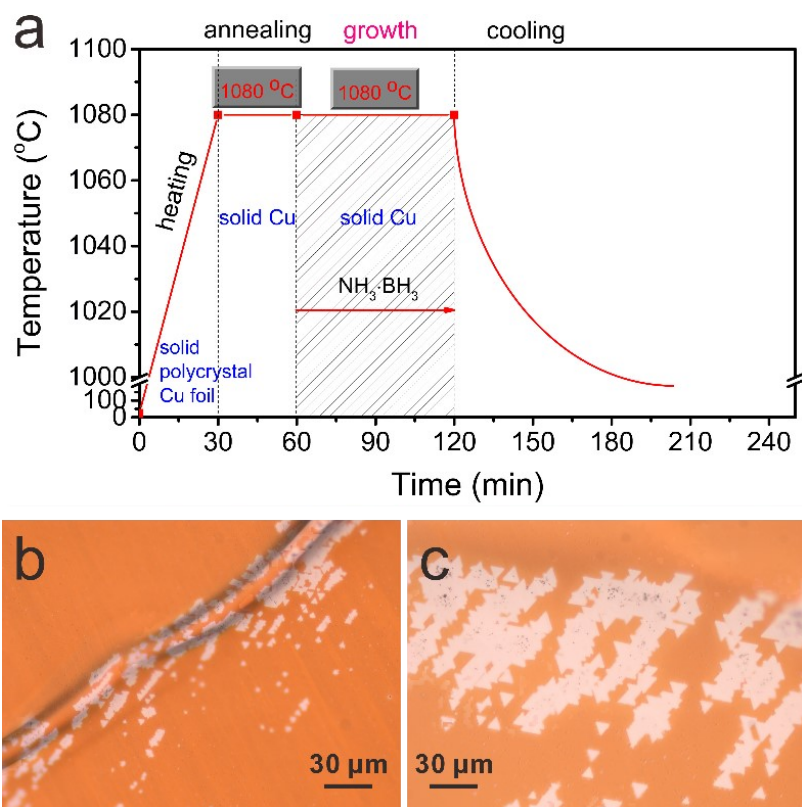


Figure S7. Nonuniform growth of hBN on annealed Cu. a) Schematic procedure for hBN growth on annealed polycrystalline Cu by DTC APCVD. b and c) Optical images of hBN domains grown preferentially along the defect sites of rough grooves and uneven rolling surfaces on annealed polycrystalline Cu, respectively.

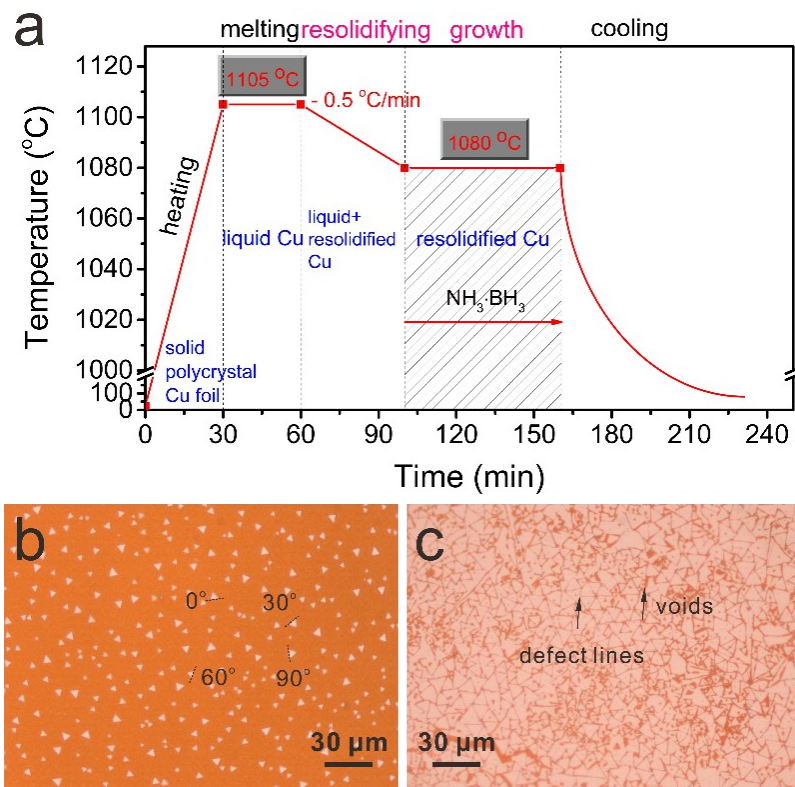


Figure S8. Misorientated growth of hBN on resolidified Cu. a) Schematic procedure for hBN growth on resolidified Cu by DTC APCVD. b and c) Optical images of hBN domains and films grown on resolidified Cu, respectively.

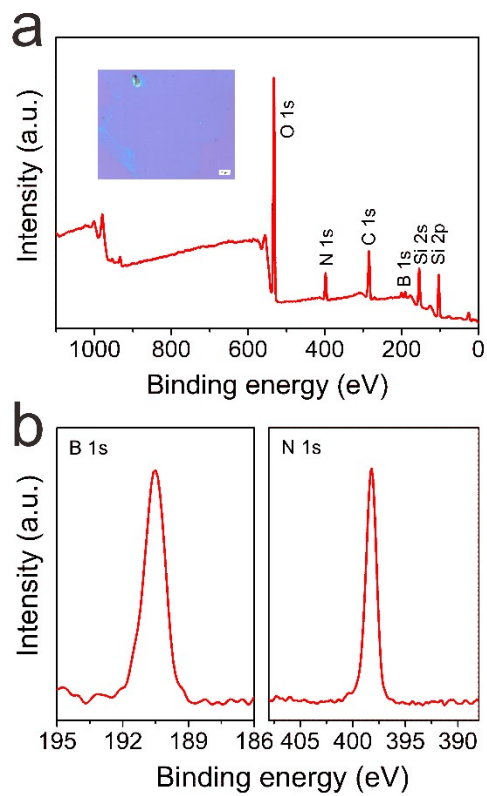


Figure S9. Stoichiometry of B and N in hBN film grown on liquid Cu by DTC APCVD. a) Survey XPS spectrum, b) B 1s and N 1s core level spectra. The inset in a) shows the optical image of the transferred hBN film on SiO₂/Si for XPS measurement.

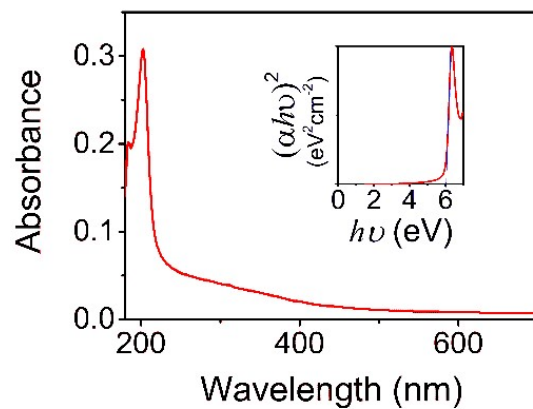


Figure S10. UV-Vis absorption spectrum of the transferred hBN film on quartz plate. The inset shows the plot of $(\alpha h\nu)^2$ versus $h\nu$, by which the optical band gap of 6.0 eV for hBN film is determined.

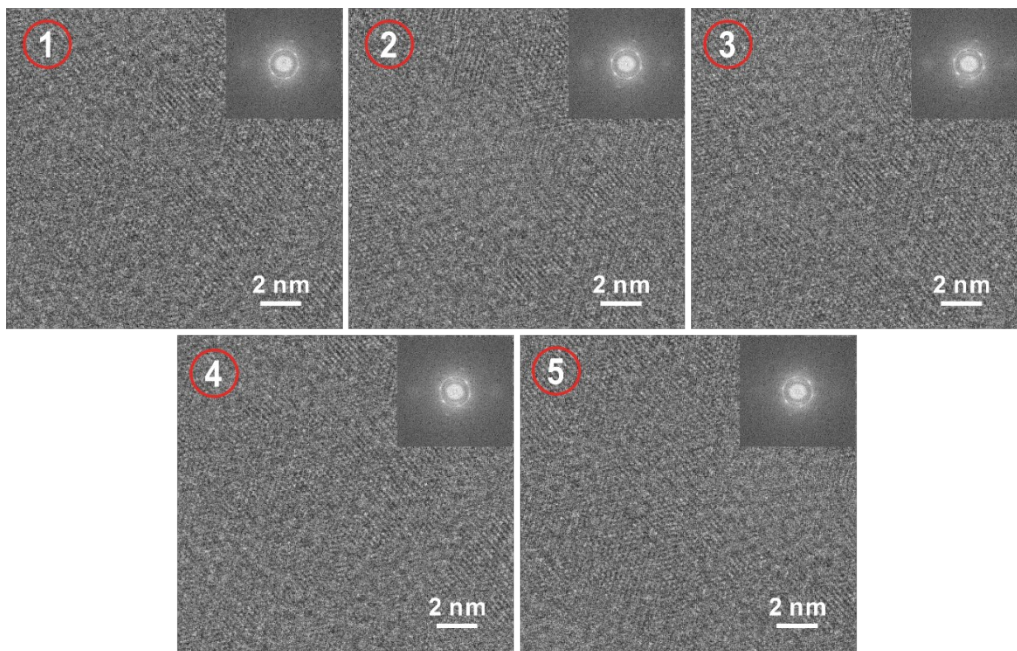


Figure S11. HRTEM images of the regions numbered 1-5 in Fig. 4a. The insets in each images show the corresponding fast Fourier transform patterns.

Table S1 Comparison of our hBN with other reports on hBN synthesis.

Strategy	Growth method	Growth mechanism	Substrate	T (°C)	Film (domain) size	Uniform alignment control of each domain before merging	hBN/substrate lattice, pattern registry dependency	Single-crystal	Ref.
Suppressing nucleation	LPCVD	Domain enlarging	Cu-Ni	1050-1090	130 μm	Yes, 100% need.	Yes	Yes (domain)	19
	LPCVD	Domain enlarging	Electropolished Cu enclosure	1050	300 μm	Yes, 100% need.	Yes	Yes (domain)	21
	IBSD	Domain enlarging	Ni (111)	1050	600 μm	Yes, 100% need.	Yes	Yes (domain)	22
Multi nuclei stitching	LPCVD	Seam stitching	Annealed poly. Cu	1035	-	Yes, 100% need.	Yes	No (film)	38
	APCVD	Seam stitching	Solidified Cu (110)	1075	2×1.5 cm ²	Yes, 100% need.	Yes	No (film)	35
	APCVD	Seam stitching	Liquid Cu	1110	-	Not need.	No	No (film)	28
	APCVD	Seam stitching	Liquid Cu	1110	-	Not need.	No	No (film)	27
	LPCVD	Edge-coupling-guided seamless stitching	Cu (110) vicinal surface	1035	10×10 cm ²	Yes, 100% need.	Yes	Yes (film)	24
	LPCVD	Edge-coupling-guided seamless stitching	Cu (111) vicinal surface	1050	2 inch	Yes, 100% need.	Yes	Yes (film)	12
	APCVD	Self-collimated seamless stitching	Liquid Au	1100	3×3 cm ²	Not need.	No	Yes (film)	7
	APCVD	Self-aligned stitching	Liquid Cu	1105	1×1 cm ²	Not need.	No	quasi-single-crystal (film)	This work

Note: LPCVD-low-pressure CVD; IBSD-ion beam sputtering deposition; APCVD-atmospheric pressure CVD.